Astron. Astrophys. 266, 463–478 (1992)

ASTRONOMY AND ASTROPHYSICS

The abundance of nitric oxide in molecular clouds

M. Gerin[1,2], Y. Viala[2], F. Pauzat[1,2], and Y. Ellinger[1,2]

[1] Radioastronomie Millimétrique, UA336 du CNRS, École Normale Supérieure, 24 rue Lhomond, F-75231 Paris Cedex 05, France
[2] DEMIRM, UA 336 du CNRS, Observatoire de Meudon, F-92195 Meudon Cedex, France

Received April 19, accepted June 10, 1992

Abstract. We have detected two rotational transitions of nitric oxide (NO) in six molecular clouds: at two positions in the dark cloud L134N and in five giant clouds, OMC1, W51, SgrB2, SgrA $+20\ km\ s^{-1}$ and $+50\ km\ s^{-1}$ clouds. In the dark cloud L134N, the NO column density is about equal to that of $C^{18}O$, resulting in an abundance relative to H_2 of about $2\,10^{-7}$. This contrasts with the case of TMC1, where nitric oxide is less abundant than $C^{18}O$ by at least a factor two. In massive clouds too, the abundance of nitric oxide is comparable to $C^{18}O$ but shows more variations from one cloud to the other.

Nitric oxide is mainly produced in the reaction $N+OH\rightarrow NO+H$ and mainly destroyed by $N+NO\rightarrow N_2+O$. A quantum chemical study of the first reaction indicates that it proceeds with no activation barrier. Steady state chemical models reproduce satisfactorily the observed abundances of NO, and of nitrogen hydrides (NH_3, N_2H^+) in the dark cloud L134N, provided that none of the above reactions has an activation barrier. However, the model produces too much cyanides (CN, HCN+HNC): the predicted abundances agree with those observed in TMC1, well known to exhibit large abundances of C–N bearing species.

Key words: molecular processes – interstellar medium: clouds – interstellar medium: molecules – radio lines: molecular: interstellar

1. Introduction

The agreement between observed and predicted values of the abundances of interstellar molecules is getting better as the sophistication of chemical models and the precision of the observations increase. Nevertheless, the models could be improved by a better knowledge of reactions initiating the chemical scheme, at the low temperatures of the interstellar medium. Though the chemical schemes are mainly based on exothermic ion–molecule reactions, a few neutral–neutral reactions play a crucial role in interstellar chemistry. Some of these reactions have been measured at room temperature, but no measurements have been performed at the low temperatures prevailing in interstellar clouds. All the information on neutral–neutral reaction rate coefficients at such low temperatures comes from quantum mechanical calculations (e.g. Graff 1989).

As shown by Herbst & Klemperer (1973), the abundance of nitric oxide is controlled by the two neutral–neutral reactions:

$$N+OH\rightarrow NO+H \qquad [1]$$

and

$$N+NO\rightarrow N_2+O. \qquad [2]$$

Recent model calculations by Pineau des Forêts et al. (1990) have shown that the chemistry of nitrogen is largely dependent on neutral–neutral reactions, especially that the formation of molecular nitrogen and ammonia is initiated by reactions [1] and [2].

Among the species participating to the first reaction, OH is widely observed in clouds and NO has been detected in OMC1 (Blake et al. 1986) and in SgrB2 (Liszt & Turner 1978) with a fractional abundance, relative to H_2, of $1\,10^{-8}$. Only one line has been tentatively assigned to HNO. Other observations of nitric oxide have been made in the dark cloud L134N (MacGonagle et al. 1990) and in star forming regions (Ziurys et al. 1991) showing that this radical is present in all types of clouds with a fractional abundance in the range $0.5–5\,10^{-8}$. This value is somewhat lower than the predictions obtained by recent chemical models (Langer & Graedel 1989; Herbst & Leung 1989; Pineau des Forêts et al. 1990). In order to reconcile the observed and computed fractional abundance of NO, Pineau des Forêts et al. suggested that reaction [1] has a small activation barrier (50 K).

The purpose of the present work is to address, in more detail, the problem of the interstellar abundance of nitric oxide both observationally and theoretically. Our observations of NO in dark clouds and in giant molecular clouds are presented in Sect. 2. The derived column densities are given in Sect. 3. Section 4 presents a theoretical study, through quantum mechanical calculations, of reaction [1], the main route to NO. The implications for the interstellar chemistry of NO and other nitrogen species are discussed in Sect. 5. Our main conclusions are summarized in Sect. 6.

2. Observations

2.1. The rotational spectrum of nitric oxide

Due to the existence of an unpaired electron, the ground electronic state of the NO molecule is a $^2\Pi$ state consisting of two substates $^2\Pi_{1/2}$ and $^2\Pi_{3/2}$. Although, strictly speaking, the energy spectrum of the ground electronic state of NO is described by a coupling of angular momenta intermediate between Hund's cases *a* and *b*, pure case a coupling gives a very good representation of the energy levels of this molecule. The spin orbit coupling constant A being positive, the $^2\Pi$ state is regular so that the lowest rotational level $J=1/2$ belongs to the $^2\Pi_{1/2}$ substate. The lowest level $J=3/2$ of the $^2\Pi_{3/2}$ substate, lying 180 K above, is rather difficult to populate at the low temperatures prevailing in

Send offprint requests to: M. Gerin (Paris address)

interstellar clouds. This explains that all transitions observed so far are transitions between levels of the $^2\Pi_{1/2}$ substate: $J' \rightarrow J'' = 3/2 \rightarrow 1/2$ (around 150 GHz) and $5/2 \rightarrow 3/2$ (around 250 GHz).

The interaction between the electronic angular momentum and the rotation of the nuclei produces a splitting (Λ-type doubling) of each rotational level J into two *single* rotational levels of opposite parity + and −. The parity of each upper and lower single rotational level changes between two successive J. There are hence two series of single rotational levels, the series of lower Λ-doubling components and the series of upper Λ-doubling components. In each series, the parity changes alternatively between two successive levels. By analogy with Σ states, the two series of levels are noted Π^+ and Π^- (also noted Π_c and Π_d in order that the sign of the series is not to be confused with the parity sign of each single rotational level). According to Herzberg (1950, p. 239), the series Π^+ (or Π_c) consists of levels $J = (2n+1)/2$ which have parity + for n even and parity − for n odd. The reverse is true for the series Π^- (or Π_d). For the $^2\Pi_{1/2}$ substate NO, the lower Λ-doubling component of the lowest rotational level ($J = 1/2$, $n = 0$) has a positive parity and hence belongs to the Π^+ series, as all lower Λ-doubling components, while the upper Λ-doubling components form the Π^- series. This ordering of single rotational levels, together with the selection rule for electric dipole transitions which states that only transitions between levels of opposite parity are allowed, lead to the existence of two series of transitions, the Π^+ and Π^- bands, connecting Π^+ and Π^- levels, respectively.

The nitrogen atom has a non zero nuclear spin ($I = 1$) so that interaction between the nuclear spin vector $\boldsymbol{I}$ and the total angular momentum $\boldsymbol{J}$ leads to a splitting of each single rotational level into *2 min* $(I, J) + 1$ hyperfine levels; each hyperfine level is characterized by a quantum number F ($\boldsymbol{F} = \boldsymbol{I} + \boldsymbol{J}$) varying from $|\boldsymbol{I} - \boldsymbol{J}|$ to $\boldsymbol{I} + \boldsymbol{J}$ and has a statistical weight $g_F = 2F + 1$. In the case of NO, hyperfine splitting is due to the interaction of both the magnetic moment and the electric quadrupole moment of the nitrogen nucleus with the electrons. Selection rules for electric dipole transitions between hyperfine levels are $\Delta J = \pm 1$ and $\Delta F = 0, \pm 1$ so that each transition between the two single rotational levels J'–$J'' = 3/2$–$1/2$ is divided into 5 hyperfine components, and each transition between levels J'–$J'' = 5/2$–$3/2$ is divided into 6 components. The microwave spectrum of NO in the ground state $^2\Pi_{1/2}$ has been measured by Gallagher & Johnson (1956) and by Saleck et al. (1991), and the spectroscopic constants have been obtained from a detailed analysis including all possible interactions and uncoupling effects. We list in Table 1 the frequencies $\nu_{J'F',J''F''}$ of all hyperfine transitions extracted from these works, between rotational levels J'–$J'' = 3/2$–$1/2$ and $5/2$–$3/2$. Figure 1

Table 1. Parameters of the hyperfine transitions of NO

Transition $J', F' \rightarrow J'', F''$	Frequency (MHz)	$S_{J'J''}$	$A_{J'J''}$ (s^{-1})	$g_{J'}$	$S_{F'F''}$	$A_{J'F',J''F''}$ (s^{-1})	$g_{F'}$	$E_{J'F'}$ (K)
Π^+ band								
3/2, 5/2→1/2, 3/2	150176.46				0.500	1.10(−7)	6	7.2070
3/2, 3/2→1/2, 1/2	150198.76				0.186	6.13(−8)	4	7.2090
3/2, 3/2→1/2, 3/2	150218.74	4/3	3.34(−7)	4	0.148	4.91(−8)	4	7.2090
3/2, 1/2→1/2, 1/2	150225.65				0.148	9.82(−8)	2	7.2103
3/2, 1/2→1/2, 3/2	150245.64				0.018	1.23(−8)	2	7.2103
Π^- band								
3/2, 1/2→1/2, 3/2	150375.30				0.018	1.23(−8)	2	7.2372
3/2, 3/2→1/2, 3/2	150439.10				0.148	4.93(−8)	4	7.2402
3/2, 5/2→1/2, 3/2	150546.46	4/3	3.34(−7)	4	0.500	1.11(−7)	6	7.2454
3/2, 1/2→1/2, 1/2	150580.55				0.148	9.89(−8)	2	7.2372
3/2, 3/2→1/2, 1/2	150644.35				0.186	6.19(−8)	4	7.2402
Π^+ band								
5/2, 7/2→3/2, 5/2	250436.84				0.445	6.14(−7)	8	19.2254
5/2, 5/2→3/2, 3/2	250440.66				0.280	5.16(−7)	6	19.2276
5/2, 3/2→3/2, 1/2	250448.53	2.4	1.84(−6)	6	0.167	4.61(−7)	4	19.2292
5/2, 3/2→3/2, 3/2	250475.42				0.053	1.47(−7)	4	19.2292
5/2, 5/2→3/2, 5/2	250482.94				0.053	9.83(−8)	6	19.2276
5/2, 3/2→3/2, 5/2	*250517.71*				0.002	6.15(−9)	4	19.2292
Π^- band								
5/2, 3/2→3/2, 5/2	*250645.77*				0.002	6.16(−9)	4	19.2739
5/2, 5/2→3/2, 5/2	250708.24				0.053	9.86(−8)	6	19.2768
5/2, 3/2→3/2, 3/2	250753.14	2.4	1.84(−6)	6	0.053	1.48(−7)	4	19.2739
5/2, 7/2→3/2, 5/2	250796.43				0.445	6.17(−7)	8	19.2811
5/2, 5/2→3/2, 3/2	250815.61				0.280	5.18(−7)	6	19.2768
5/2, 3/2→3/2, 1/2	250816.93				0.167	4.63(−7)	4	19.2739

a(−b) denotes a 10^{-b}

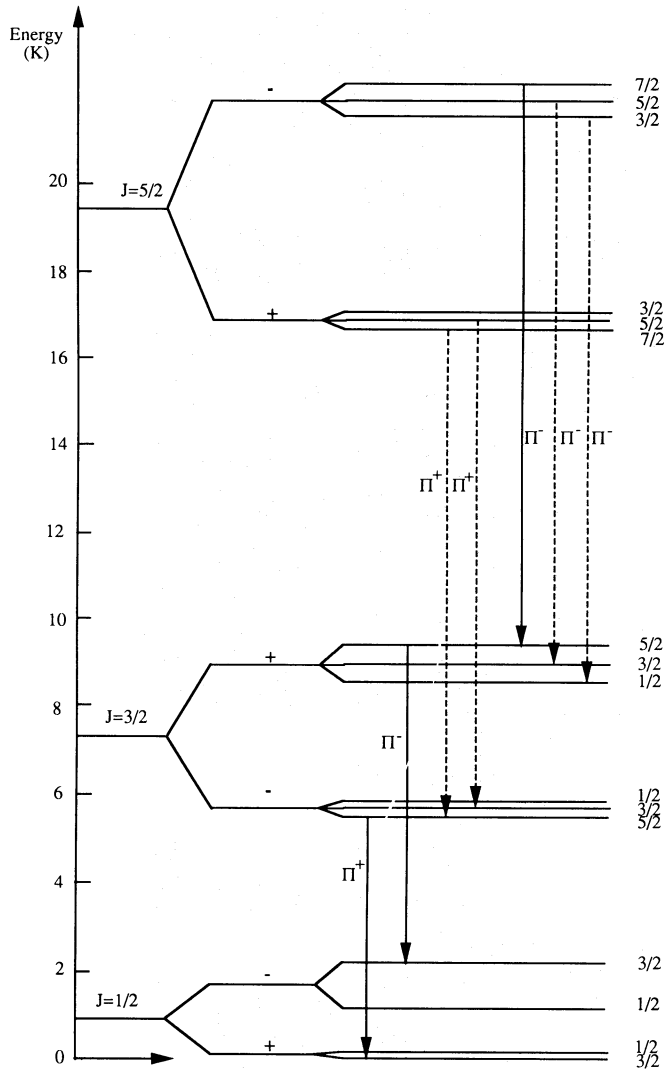

Fig. 1. Energy level diagram for NO showing the first three rotational levels of the $^2\Pi_{1/2}$ substate. To be clearly visible, the energy spacings of the hyperfine levels within a rotational level have been multiplied by 100. The observed transitions are shown on the figure as full arrows for well separated transitions and dashed arrows for blended lines

presents an energy level diagram showing the hyperfine structure of the first three rotational levels of the $^2\Pi_{1/2}$ substate. The energy spacing within a rotational level is much lower than the energy separation between two successive levels; to be visible on the figure, it has been multiplied by a factor 100. The transitions we have observed are also shown in the figure: full arrows correspond to hyperfine transitions well separated in the observed spectra, while dashed arrows indicate blended lines.

2.2. Observations

Observations were realized in July 8–9, 1989 with the IRAM 30 m telescope on Pico Veleta (Spain). We observed simultaneously the first two rotational transitions of NO, namely the $J=3/2-1/2$ and $J=5/2-3/2$ multiplets around 150.4 and 250.5 GHz. We used two SIS receivers tuned in SSB mode with a sideband rejections of 6 dB. The receiver temperatures were about 200 K (2 mm) and 450 K (1 mm), and the corresponding system temperature ranged between 450 and 900 K (2 mm), and 1100 to 3000 K (1 mm) depending on the weather conditions. At 2 and 1 mm the coupling of the telescope with moderately extended sources (smaller than 200″) is very close to that for point sources (D. Downes, private communication). Thus we present the spectra in the *Main Beam* temperature scale, with efficiencies of 0.6 (2 mm) and 0.45 (1.2 mm). Spectra were obtained mainly in the position switching mode and analysed with two 512×1 MHz back-ends. The base lines were flat, except at 250 GHz in poor weather conditions, and we subtracted linear or quadratic base lines. For the observations toward dark clouds, we also used two 128×100 kHz filter banks centered on the two main components of the 150 GHz multiplet, at 150.176 and 150.546 GHz. Unfortunately, the sky frequency was fixed during the observations at a value corresponding to L134N (this source was observed at the beginning of the run), not following the change in sky frequency as the telescope moved from one source to the other. This variation amounts to a few $\mathrm{km\,s^{-1}}$ (a few MHz). Thus the velocity and frequency scale were not reliable, but we could check the calibration and frequency with the strong H_2CO ($2_{11}-1_{10}$) line at 150.498 GHz which is well seen in most of our sources. We used this line to adjust the frequency scale. Since the NO lines are observed in the same frequency range, with good frequency spacing, we are confident that the observed lines are due to nitric oxide. At 250 GHz the NO lines are slightly blended with high energy lines of methyl formate and other species, but should contribute to most of the intensity of the detected lines since transitions of similar energy at other frequencies are weak or not detected in our spectra and in the frequency survey of OMC1 (Blake et al. 1986).

2.3. Spectra

We searched for the NO lines in a sample of well known giant and dark clouds. Table 2 lists the positions of the sources, together with the column densities of $C^{18}O$ and H_2. Figures 2 and 3 present a selection of the spectra obtained for the $J=3/2-1/2$ transition, and $J=5/2-3/2$ transition respectively. The observed main beam temperatures and integrated intensities are given in Table 3.

3. Interstellar abundance of NO

3.1. Determination of column densities

To take into account the possible different opacities of the hyperfine components and to check the identification of the lines, we have computed separately the column density of nitric oxide for each hyperfine component.

Assuming that the emission line $J', F'\rightarrow J'', F''$ is optically thin, the column density of NO molecules in the upper level J', F' can be obtained from the integrated area of the brightness temperature over the line:

$$N(J',F')=\frac{8\pi k}{hc^3}\frac{\nu^2_{J'F',J''F''}}{A_{J'F',J''F''}}\frac{10^5}{(1-J_{\nu_0}(T_{\mathrm{BG}})/J_{\nu_0}(T_{\mathrm{ex}}))}\int T_{\mathrm{R}}\,\mathrm{d}V, \qquad (1)$$

where

$$J_{\nu_0}(T)=\frac{h\nu_0}{k}\frac{1}{\exp\left(\frac{h\nu_0}{kT}\right)-1}, \qquad (2)$$

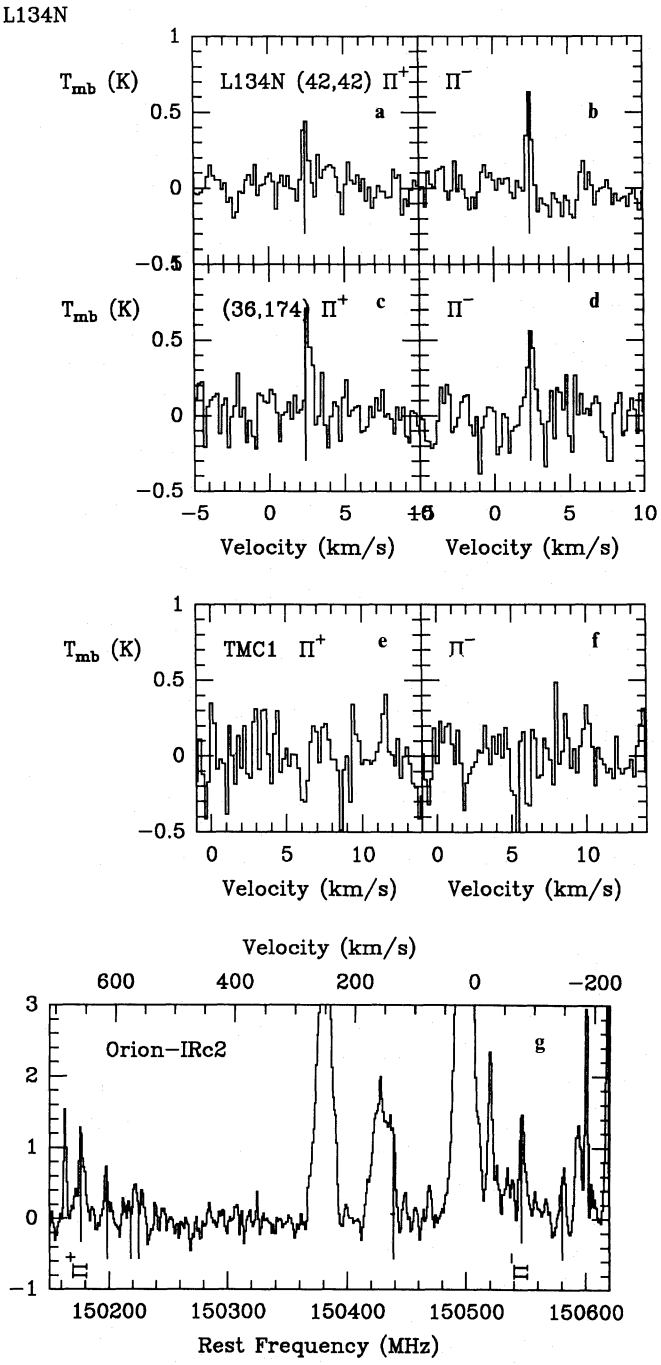

Fig. 2a–g. Spectra of the 3/2–1/2 transition of NO, the temperature scale is T_{mb} in Kelvins. Lines are drawn at the expected frequency of the NO lines. **a** $\Pi^+ 5/2-3/2$ component towards L134N (42″, 42″), **b** $\Pi^- 5/2-3/2$ towards L134N (42″, 42″); **c** and **d** same transitions as **a** and **b** towards L134N (36″, 174″); **e** and **f** same transitions as **a** and **b** towards TMC1; **g** the NO multiplet towards Orion-IRc2. The lower scale is the rest frequency in MHz assuming a LSR velocity of 8 km s^{-1} for the H_2CO line at 150 498 MHz, the upper scale the LSR velocity

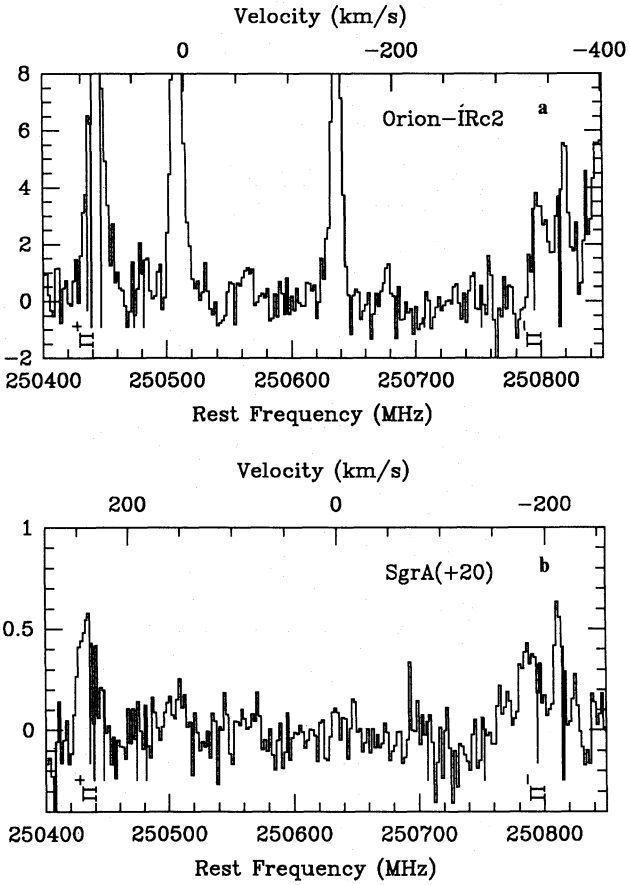

Fig. 3a and b. Spectra of the 5/2–3/2 transition of NO, the lower scale is the rest frequency in MHz, the upper scale the LSR velocity, the temperature scale is T_{mb} in Kelvins. Lines are drawn at the expected frequency of the NO lines. **a** Orion-IRc2. **b** SgrA +20

and $T_{BG}=2.7$ K is the temperature of the background radiation, T_{ex} is the excitation temperature of the transition and $\nu_0=\nu_{J'F',J''F''}$. The transition probability between two hyperfine levels is given by

$$A_{J'F',J''F''}=\frac{64\pi^4}{3hc^3}\nu^3_{J'F',J''F''}\frac{\mu^2}{2F'+1}S_{J'J''}S_{F'F''}, \quad (3)$$

where $S_{J'J''}$ is the rotational line strength and $S_{F'F''}$ is a dimensionless factor which obeys the sum rules:

$$\sum_{F'}\sum_{F''}S_{F'F''}=1, \quad \sum_{F''}S_{F'F''}=\frac{2F'+1}{(2I+1)(2J'+1)},$$

$$\sum_{F'}S_{F'F''}=\frac{2F''+1}{(2I+1)(2J''+1)}. \quad (4)$$

Expressions of "hyperfine" line strengths obeying these sum rules have been given by Tatum (1986). The sum of the transition probabilities of the lines connecting all hyperfine levels between two single rotational levels J' and J'' is equal to the transition probability $A_{J'J''}$ between these two rotational levels:

$$A_{J',J''}=\frac{64\pi^4}{3hc^3}\nu^3_{J',J''}\frac{\mu^2}{2J'+1}S_{J'J''}. \quad (5)$$

For pure Hund's coupling case *a*, the rotational line strength for a transition $J+1\rightarrow J$ between two single rotational levels of a $^2\Pi_{1/2}$ state [branch $R_1(J)$], which is the case of all transitions

Table 2. List of sources

Name	α(1950)	δ(1950)	V_{LSR} (km s^{-1})	N($C^{18}O$) (cm^{-2})	N(H_2)[a] (cm^{-2})	References
TMC1	04:38:38.6	25:35:45	5.8	$2.0\,10^{15}$	$1.2\,10^{22}$	1
Orion-IRc2	5:32:47.0	−5:24:24	9.0	$4.8\,10^{16}$	$2.8\,10^{23}$	2
L134N	15:51:30.0	−2:43:31.0				
	(42″, 42″)		2.5	$1.0\,10^{15}$	$5.9\,10^{21}$	3
	(36″, 174″)		2.5	$1.1\,10^{15}$	$6.5\,10^{21}$	3
SgrA(+20)	17:42:29.4	−29:03:31	15	$1.5\,10^{16}$	$8.8\,10^{22}$	4
SgrA(+50)	17:42:40	−28:58:20	50	$5.0\,10^{16}$	$2.9\,10^{23}$	4
SgrB2(OH)	17:44:11.0	−28:22:30	60	$7.7\,10^{16}$	$4.0\,10^{23}$	5
W51D	23:11:36.5	61:11:50	57	$1.2\,10^{17}$	$7.0\,10^{23}$	6

[a] The column densities of H_2 are deduced from those of $C^{18}O$ assuming the same fractional abundance $1.7\,10^{-7}$ as given by Frerking et al. 1982.
References: 1. Schloerb & Snell 1984; 2. Wilson et al. 1986; 3. Swade 1989; 4. Gerin et al. 1990; 5. Lis & Goldsmith 1989; 6. Mauersberger et al. 1989.

Table 3. Results

Transition $J'F' \rightarrow J''F''$	T_{mb} (K)	Area (K km s^{-1})	Nu (10^{14} cm^{-2})	N_{tot} (10^{14} cm^{-2})	T_{ex} (K)	[$C^{18}O$]/[NO]
L134N (42″, 42″)						
3/2, 5/2−1/2, 3/2 (Π^+)	0.48	0.22	0.95	9.9	10	0.9
3/2, 5/2−1/2, 3/2 (Π^-)	0.64	0.27	1.2	12	10	
L134N (36″, 174″)						
3/2, 5/2−1/2, 3/2 (Π^+)	0.67	0.32	1.4	14	10	0.76
3/2, 5/2−1/2, 3/2 (Π^-)	0.57	0.33	1.4	15	10	
TMC1						
3/2, 5/2−1/2, 3/2 (Π^+)	<0.21	<0.20	<0.86	<9.0	10	>2.5
3/2, 5/2−1/2, 3/2 (Π^-)	<0.30	<0.15	<0.64	<6.7	10	
Orion-IRc2						
3/2, 5/2−1/2, 3/2 (Π^+)	1.4	15	61	810	20	0.56
3/2, 5/2−1/2, 3/2 (Π^-)	1.1	17	70	920	20	
5/2, 7/2−3/2, 5/2 (Π^+)b	6.9	58	63	650	20	
5/2, 5/2−3/2, 3/2 (Π^+)b						
5/2, 7/2−3/2, 5/2 (Π^-)	4.7	35	70	1300	20	
5/2, 5/2−3/2, 3/2 (Π^-)b	4.7	35	44	640	20	
5/2, 3/2−3/2, 1/2 (Π^-) b						
W51D						
3/2, 5/2−1/2, 3/2 (Π^+)	0.17	1.8	7.7	81	10	12
3/2, 5/2−1/2, 3/2 (Π^-)	0.25	2.8	12	130	10	
5/2, 7/2−3/2, 5/2 (Π^+)b	0.62	5.7	6.3	94	10	
5/2, 5/2−3/2, 3/2 (Π^+)b						
5/2, 7/2−3/2, 5/2 (Π^-)	0.65	3.6	7.3	190	10	
5/2, 5/2−3/2, 3/2 (Π^-)b	0.55	3.1	4.0	83	10	
5/2, 3/2−3/2, 1/2 (Π^-)b						
SgrB2 (OH)						
3/2, 5/2−1/2, 3/2 (Π^+)	0.45	9.2	37	790	40	1.1
3/2, 5/2−1/2, 3/2 (Π^-)	0.57	6.8	27	580	40	
5/2, 7/2−3/2, 5/2 (Π^-)	0.78	19	38	820	40	
5/2, 5/2−3/2, 3/2 (Π^-)b	0.65	16	20	350	40	
5/2, 3/2−3/2, 1/2 (Π^-)b						

Table 3 (continued)

Transition $J'F' \rightarrow J''F''$	T_{mb} (K)	Area (K km s^{-1})	Nu (10^{14} cm^{-2})	N_{tot} (10^{14} cm^{-2})	T_{ex} (K)	[C^{18}O]/[NO]
SgrA (+20)						
3/2, 5/2–1/2, 3/2 (Π^+)	0.28	4.5	19	220	15	0.83
3/2, 5/2–1/2, 3/2 (Π^-)	0.18	3.0	12	140	15	
5/2, 7/2–3/2, 5/2 (Π^+)b	0.56	8.8	9.6	110	15	
5/2, 5/2–3/2, 3/2 (Π^+)b						
5/2, 7/2–3/2, 5/2 (Π^-)	0.44	7.3	15	280	15	
5/2, 5/2–3/2, 3/2 (Π^-)b	0.45	7.6	9.6	150	15	
5/2, 3/2–3/2, 1/2 (Π^-)b						
SgrA (+50)						
3/2, 5/2–1/2, 3/2 (Π^+)	0.67	10	43	450	10	1.2
3/2, 5/2–1/2, 3/2 (Π^-)	0.80	8.1	36	360	10	
5/2, 7/2–3/2, 5/2 (Π^+)b	0.76	14	15	230	10	
5/2, 5/2–3/2, 3/2 (Π^+)b						
5/2, 7/2–3/2, 5/2 (Π^-)	0.78	15	31	800	10	
5/2, 5/2–3/2, 3/2 (Π^-)b	0.49	9.7	12	260	10	
5/2, 3/2–3/2, 1/2 (Π^-)b						

b: blended lines

considered here, is given by (e.g. Bennett 1970):

$$S_{J+1,J}=\frac{(2J+3)(2J+1)}{4(J+1)}. \quad (6)$$

A much more complicated expression holds for intermediate coupling between case *a* and *b* (Bennet 1970); in the case of NO, both expressions gives the same value of the rotational line strength to better than 1%.

The rotational and hyperfine line strengths, the transition probabilities for rotational transitions $A_{J'J''}$ and hyperfine transitions $A_{J'F',J''F''}$ and the statistical weights of upper levels $g_{J'}$ and $g_{F'}$ are also given in Table 1 for all hyperfine transitions between rotational levels $J'-J''=3/2-1/2$ and $5/2-3/2$ of the $^2\Pi_{1/2}$ substate of NO. The transition probabilities have been computed by using the value $\mu=0.15872$ D for the dipole moment of NO (Poynter & Pickett 1984).

Computation of column densities in separate hyperfine levels $N(J', F')$ and of total column densities N_{tot} requires the knowledge of excitation temperatures of the observed transitions. The total column density of the molecule N_{tot}, which is the only relevant quantity to be compared with results from chemical models, must be derived by summing over all levels that can be efficiently populated in interstellar clouds. The simplest and most commonly adopted method to do that, is to assume that the excitation of molecules is entirely dominated by collisional processes so that the population of levels obeys the Boltzman law at the kinetic temperature of the cloud, T_{kin}. With this assumption, the total column density of the molecule including all levels, can be obtained from the column density $N(J', F')$ in a particular level using the relation:

$$N_{tot}=\frac{N(J',F')}{g_{F'}}Q_{rot}(T_{kin})\exp\left[\frac{E(J',F')}{kT_{kin}}\right], \quad (7)$$

where Q_{rot} is the rotational partition function, defined as

$$Q_{rot}(T)=\sum_{\Sigma}\sum_{p}\sum_{J,F} g_F \exp\left[-\frac{E(J,F)}{kT}\right]. \quad (8)$$

The first summation is over all substates of the ground electronic state and the second takes into account the possible existence of two series of single rotational levels of opposite parity. The rotational partition function of NO has been computed through explicit summation over all hyperfine levels belonging to the 50 first rotational levels of both substates $^2\Pi_{1/2}$ and $^2\Pi_{3/2}$. The contribution of the $^2\Pi_{3/2}$ substate is negligible below 100 K.

For the case of nitric oxide, we assumed that the lines are optically thin and thermalized: the Einstein coefficients for the 5/2–3/2 and 3/2–1/2 transitions are rather small (Table 1). Therefore these transitions require H_2 densities greater than a few 10^3 cm^{-3} for thermalization $T_{ex}\approx T_{kin}$, which are present in all observed clouds.

Table 3 also lists the values of the column density in the upper energy level of each hyperfine component (column 4) and the total column density of nitric oxide (column 5) assuming an excitation temperature T_{ex} as given in column 6, and a kinetic temperature equal to T_{ex}. For blended lines, we summed the Einstein coefficients of the hyperfine components to deduce the column density in the upper level, and summed the weights $g_{F'}$ to obtain the total column density N_{tot} [cf. Eqs. (1), (3) and (7)].

We adjusted the values of T_{ex} by comparing the values of N_{tot} deduced from the 3/2–1/2 and the 5/2–3/2 transitions. The upper energy levels of these transitions lie at 7.2 and 19.2 K above the fundamental, thus these observations are not sensitive to temperatures greater than about 40 K. The rotational temperatures range between 10 and 40 K, all values which are likely present in these sources, but which do not correspond to the hottest points. This difference is particularly clear towards Orion-IRc2 and W51D, since these sources are thought to be warmer than 20 K, even for the interstellar medium not directly associated with the young star (hot core) which may be heated up to 200 K. It should be noted, however, that we have performed this comparison without correcting for the different sizes of the beam at 150 and 250 GHz. For sources associated with star formation, there are density and temperature gradients in the beam, which cannot be taken into account without maps of the

same extent in the two lines. Our procedure may underestimate the excitation temperature and the column density for sources smaller than the telescope beam at 150 GHz (HPBW = 16″).

For IRc2 and W51D, we have some indications that the emission of nitric oxide is peaked towards the observed position: mispointed observations of IRc2 presenting a faint H_2CO line present also faint NO lines varying in the same way as H_2CO. At offset (−15″, −15″) in the W51D cloud the formaldehyde line is still observed, but the nitric oxide lines are weak or absent. Furthermore, the intensities reported by Ziurys et al. (1991) towards IRc2 and corrected for beam efficiency are fainter than ours, suggesting that the emission is peaked in a region smaller than their 41″ beam.

This difficulty is not so severe for the dark clouds L134N and TMC1, or for the warm clouds near the Galactic Center, where the kinetic temperature is more uniform across the beam and along the line of sight.

The last column of Table 3 gives the ratio of column densities of NO and $C^{18}O$, two species with similar dipole moment and fractional abundance. The references for the observations of $C^{18}O$ are given in Table 2. They are taken with a beam as comparable as possible to the 16″ beam of the 30 m telescope at 150 GHz, but in most cases the resolution is lower in $C^{18}O$ than in NO. The two dark clouds behave differently: $C^{18}O/NO \approx 0.9$ for L134N and >2.5 for TMC1. The observations of the other sources are less homogeneous. Nevertheless, the column densities of $C^{18}O$ and NO are nearly equal for the clouds close to the Galactic Center; the abundance of NO in the two star forming clouds being affected by the unknown source size. Assuming a fractional abundance of $C^{18}O$ relative to H_2 of $1.7\,10^{-7}$ as determined by Frerking et al. (1982), the fractional abundance of NO is about $2\,10^{-7}$ in L134N. For the other clouds, the fractional abundance of $C^{18}O$ is less known: towards the Galactic Center the isotopic ratio are modified and the species are also condensed on the grains (Lis & Goldsmith 1989) suggesting that the fractional abundance of $C^{18}O$ decreases from $1.7\,10^{-7}$ to $\leq 1\,10^{-7}$. The abundance of nitric oxide seems to follow that of $C^{18}O$. Orion IRc2 is the line of sight presenting the highest NO column density relative to $C^{18}O$: the fractional abundance of nitric oxide is $\geq 3\,10^{-7}$ much higher than the values obtained with the chemical models which predict a decrease of NO abundance as the density increases. The lines are peaked on the molecular core suggesting that shocks and grain chemistry may affect the abundance of nitric oxide, in the same way as they affect the abundance of ammonia, methanol and others molecules.

These observations demonstrate that nitric oxide is a fairly abundant interstellar molecule, *the most abundant nitrogenated species so far detected in dark and warm clouds.* With this high interstellar abundance and the key role of nitric oxide in nitrogen chemistry, it is important to study the reaction scheme in more detail.

The interstellar chemistry of nitrogen has recently been reviewed by Pineau des Forêts et al. (1990), following the recognition that the two reactions which were supposed to initiate the nitrogen chemistry are inefficient. The first one: $H_3^+ + N \rightarrow NH_2^+ + H$ has an activation barrier (Herbst et al. 1987). The second one: $N^+ + H_2 \rightarrow NH^+ + H$ has been studied in the laboratory down to $T = 8$ K (Marquette et al. 1988) and appears to be slightly endothermic, by 169 K with H_2 ($J=0$) and by 43 K with H_2 ($J=1$). The endothermicity with ortho-H_2 is not so large and, as shown by Le Bourlot (1991) and as already taken into account by Viala (1986), provided the ortho-H_2/para-H_2 ratio is larger than 10^{-4}, the reaction can drive the formation of nitrogen hydrides up to NH_3, but it can no longer be considered as the first step of nitrogen chemistry since the only efficient way to produce N^+ is the reaction: $He^+ + N_2 \rightarrow N^+ + H + He$, which requires the presence of N_2. Pineau des Forêts et al. (1990) have shown that N_2 is mainly produced by reaction [2]. Thus reactions [1] and [2] initiate the whole nitrogen chemistry.

4. Study of the reaction leading to nitric oxide

While reaction $N + NO \rightarrow N_2 + O$ [2] is one of the two initiating reactions in the formation of the interstellar nitrogen molecule (Pineau des Forêts et al. 1990), it also plays an important role in the chemistry of the upper atmosphere, in the sense that it is a sink for NO for altitudes above 40 km (Strobel 1971; Brasseur & Nicolet 1973). Consequently, it has been widely studied experimentally and absolute reaction rates have been obtained for temperatures ranging from 196 to 670 K (Clyne & McDermid 1974; Lee et al. 1978), classical extrapolations being made for interstellar temperatures.

By contrast, reaction [1] $N + OH \rightarrow NO + H$ has not received much attention, although it is believed to be the determining step in the formation of NO, and the existing studies are contradictory. A possibility is the existence of a barrier which impedes the reaction efficiency under the conditions of the interstellar medium but is too small to be noticeable at usual experimental temperature. Thus, theoretical calculations could be useful in solving the question. Although there have been a number of previous theoretical investigations of this triatomic (H, N, O) system (Bruna & Marian 1979; Bruna 1980; Heiberg & Almlof 1982; Walch & Rohlfing 1990), all these studies are incomplete for our goal, not being intended for astrophysical purpose. However, helpful comparisons may be done with parts of our work.

We present here a full ab-initio study of reaction [1], together with the possible path of isomerization which may lead to HNO, a molecule reported in space by Ulich et al. (1977) and recently confirmed in SgrB2 (Hollis et al. 1992, in prep, quoted by Ziurys et al. 1991).

4.1. *Computational approach*

According to the energetical requirements of chemical reactions in space, all compounds in reaction

$$N(^4S) + OH(^2P) \rightarrow NO(^2P) + H(^2S)$$

are to be taken in the ground state; no photochemical process, indeed, is expected for this system, according to the astrophysical models. Among the possible surfaces, ($^3A'$, $^3A''$, $^5A'$, $^5A''$) on the reactant side and ($^1A'$, $^1A''$, $^3A'$, $^3A''$) on the product side, only triplet surfaces satisfy a direct correlation pattern. Previous work on HNO and NOH isomers (Bruna & Marian 1979; Bruna 1980; Walch & Rohlfing 1990) shows that NOH, a possible intermediate in the reaction, has a $^3A''$ ground state. Ab initio multiconfiguration Hartree–Fock (MCSCF) and configuration interaction (CI) calculations were then designed to characterize the essential feature of the $^3A''$ surface. The $^1A'$ surface was also investigated in detail because of a possible triplet to singlet transition that would lead to HNO. For the same purpose, we have also considered the rearrangement of NOH to HNO on both the triplet and singlet surfaces.

Classical valence bond structures of reactants and products are shown in Fig. 4. The dots and crosses represent those elec-

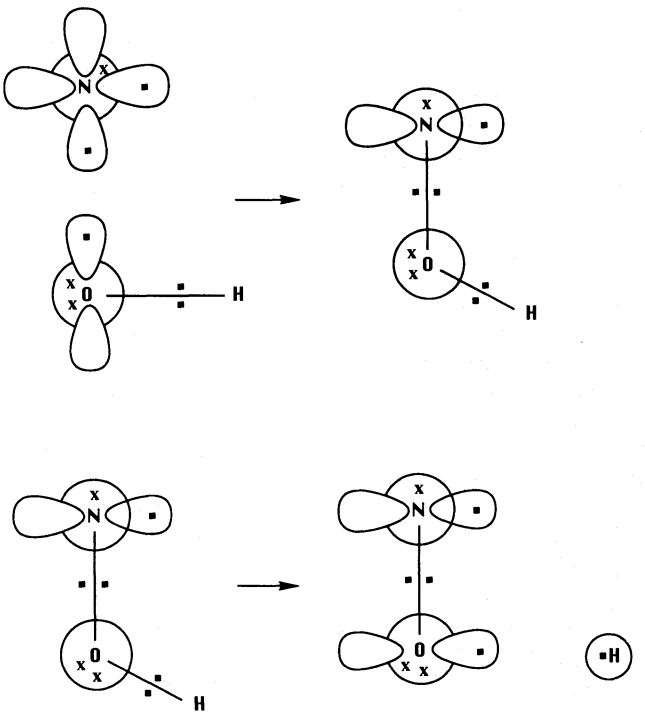

Fig. 4. Classical valence bond structures of reactants and products in the reaction N+OH→NO+H[1]. Dots represent electrons σ and crosses electons π participating in the chemical processes

trons (respectively σ and π) which participate actively in the chemical process. During the attack of the nitrogen atom onto the hydroxyl radical, on p electron of N couples with the unpaired electron on OH, and the other two p electrons of nitrogen remained unpaired to form the triplet configuration of NOH. The π electron pair on O is not actively involved in the bond formation and one can expect an attractive surface going smoothly from the reactants to NOH. Any other approach would imply an interaction with the oxygen lone pair resulting in a repulsive surface. During the destruction of NOH, the two electrons in the OH bond will unpair; one electron stays with the hydrogen atom, and the other electron forms a bonding π orbital with the unpaired electron of nitrogen lying in the molecular plane. There is a strong electronic reorganization in this process and because the loss of energy in breaking a strong σ bond (OH) overpasses the gain resulting from the formation of a weaker π bond, one may assume the existence of a barrier along the second step of the reaction.

From the above discussion, it is seen that the orbitals most actively involved in the process consist in the three p orbitals on N and O together with the 1s orbital on H. We note also that all p electrons on nitrogen and oxygen should be treated equivalently in the wave function of the diatomic molecules to account for their $^2\Pi$ symmetry. This analysis makes it possible to design a series of calculations in which the quality of the wavefunction is systematically improved from well defined theoretical plateaus.

A MCSCF wavefunction which includes all the configurations obtained by distributing eight valence electrons among these seven active orbitals in all possible ways consistent with triplet spin and overall A″ symmetry provides a correct description of the reactants, intermediate transition states and products of the reaction. This wavefunction, hereafter referred to as CAS, contains 298 and 260 configuration state functions (CSF) for ^{3}A″ and ^{1}A′ states and was used mainly for exploratory calculations.

To realize a more accurate description of the electronic rearrangements, we carried out larger MCSCF calculations, hereafter referred to as CASL, including the four 2s electrons in the active space; this, in order to get a better description of the rehybridization that occurs in highly bent structures, especially the transition state for the hydrogen transfer from NOH to HNO. This configuration space contains 1722 CSFs for the ^{3}A″ surface. A parallel investigation of the ^{1}A′ surface was performed using the corresponding 1316 CSFs singlet space.

In the third plateau, the natural orbitals of these latter calculations were then used in a first order configuration interaction treatment. The CASL space was extended by adding all configurations obtained by distributing eleven electrons in the active space and one electron in the external orbitals, and able to fulfill the ^{3}A″ spin and symmetry requirements. This FOCI n-particle space includes 129 486 CSFs and 80 612 CSFs for the ^{3}A″ and ^{1}A′ states respectively.

All the calculations reported here were done with a double zeta plus polarization (DZP) basis set (Mc Lean et al. 1977), using ALCHEMY computer codes (Lengsfield 1980; Lengsfield & Liu 1981; Liu & Yoshimine 1981).

4.2. Results and deductions

The final optimized CASL structures of the stationary points are reported in Table 4; HNO (^{1}A′) which is the most stable point of the triatomic system is also reported for comparison. Energies and dipole moments are presented in Table 5 for all wavefunctions using the CASL orbitals.

Comparison of the calculated structure with experiment (NO = 1.211 Å; NH = 1.062 Å); <HNO = 108°5 taken from Dalby (1958) shows that the bond lengths are overestimated by about 0.002 Å. This is typical of valence CASSCF calculations which are known to emphasize left-right correlation systematically. Consequently, the geometrical parameters given in this paper should not be taken for identification purposes without being properly corrected.

Concerning potential energy surfaces, quantities of interest are given in Fig. 5. It can be seen that:

— there is no activation energy on the way to intermediate NOH (^{3}A″); an extensive mapping of the region where the activation barrier may be expected on the entrance channel did not show any inversion of the gradient of the potential upon increasing the quality of the wavefunction.

— a barrier opposes dissociation on the exit channel but the energy released in the formation of NOH (62 kcal mol^{-1}) is large enough to lead to final products since the barrier opposing dissociation is only 34 kcal. The overall process is exothermic by 41 kcal. The 28 kcal ($\approx$14 000 K) difference between the reactants and the top of the barrier is large enough to avoid the temperature dependence problems (Herbst et al. 1991) and the possible influence of low lying rotational and vibrational levels (Graff & Dalgarno 1987), characteristic of small barriers. However, the existence of a stable NOH (^{3}A″) in molecular clouds cannot be rejected and, taking into account the dipole moment value, observations might be possible. Furthermore, the reverse reaction of H onto NO will not yield to NOH in view of the 13 kcal activation barrier but give HNO (^{1}A′).

Table 4. CASL structures for N+OH $^3A''$ and $^1A'$ stationary points

System[a]	r_{NO}	r_{OH}	r_{NH}	α_{NOH}	α_{HNO}	E_{CASL}
N (^4S)+OH ($^2\Pi$)		0.981				−129.82826
NO ($^2\Pi$)+H (^2S)	1.174					−129.89286
NOH ($^3A''$)	1.363	0.978		104.96		−129.90834
TS[b] ($^3A''$)	1.222	1.421		115.69		−129.85745
HNO ($^3A''$)	1.249		1.040		117.33	−129.91176
RSD[c] ($^3A''$)	1.357	1.209		56.00		−129.84942
NOH ($^1A'$)	1.285	0.999		109.25		−129.88660
TS[b] ($^1A'$)	1.201	1.267		117.52		−129.87586
HNO ($^1A'$)	1.224		1.078		108.40	−129.95704
RSD[c] ($^1A'$)	1.360	1.112		61.93		−129.83889

[a] Bond lengths in Angströms, angles in degrees, energies in a.u (1 a.u. ≈ 3.14 10^5 K).
[b] Transition state along the dissociative coordinate N–OH.
[c] Rearrangement saddle point for the internal hydrogen migration.

Table 5. Energies and dipole moments for CASL structures for N+OH $^3A''$ and $^1A'$ stationary points at CASL and first order CI levels

System[a]	CASL		FOCI	
	E	μ	*E*	μ
N (^4S)+OH ($^2\Pi$)	−129.82826	1.769	−129.92393	1.669
NO ($^2\Pi$)+H (^2S)	−129.89284	0.148	−129.98944	0.143
NOH ($^3A''$)	−129.90834	2.033	−130.02286	1.993
TS[b] ($^3A''$)	−129.85145	0.646	−129.96795	0.824
HNO ($^3A''$)	−129.91176	1.924	−130.02743	1.847
RSD[c] ($^3A''$)	−129.84942	1.368	−129.96724	1.299
NOH ($^1A'$)	−129.88661	2.711	−129.98571	2.511
TS[b] ($^1A'$)	−129.87586	0.904	−129.98275	0.670
HNO ($^1A'$)	−129.95704	1.634	−130.06007	1.531
RSD[c] ($^1A'$)	−129.83889	1.752	−129.94636	1.601

[a] Energies in a.u. (1 a.u. ≈ 3.14 10^5 K), dipole moments in debyes.
[b] Transition state along the dissociative coordinate N–OH.
[c] Rearrangement saddle point for the internal hydrogen migration.

In view of the large exothermicity of NOH formation, we also considered the possible isomerization of NOH to HNO, the hydrogen atom shifting from O to N on the triplet surface. The transition state of this process has a triangular geometry (see Table 4). However, although the reaction may lead to NOH as an intermediate, it can be seen that this intermediate will not rearrange to HNO because the activation barrier for this process is higher than the dissociation energy to the products. The possible route to HNO remaining in this process implies a triplet to singlet transition which is efficient only via spin-orbit coupling. Using Ha & Cimiraglia (1982) formalism to evaluate the spin orbit element, one obtains a life time of 1 second for the triplet state which means that HNO cannot be reached in this process. Finally, coming from initial products (N+OH), none of the routes to HNO is possible.

The main conclusion of these calculations is that no significant activation barrier opposes formation of NO ($\leq$ 50 K on the entrance channel, 0 K on the exit channel). However, when taking into account the accuracy of our calculations, the possibility of finding an activation barrier of a few tens of kelvins on the entrance channel cannot be ruled out and its influence on models has to be tested.

5. Implications for interstellar chemistry

5.1. The abundances of nitrogenated molecules

The dark cloud L134N has been extensively studied by Swade (1989), who observed several species at the positions where we detected NO. Despite the difference in beam sizes, we present in

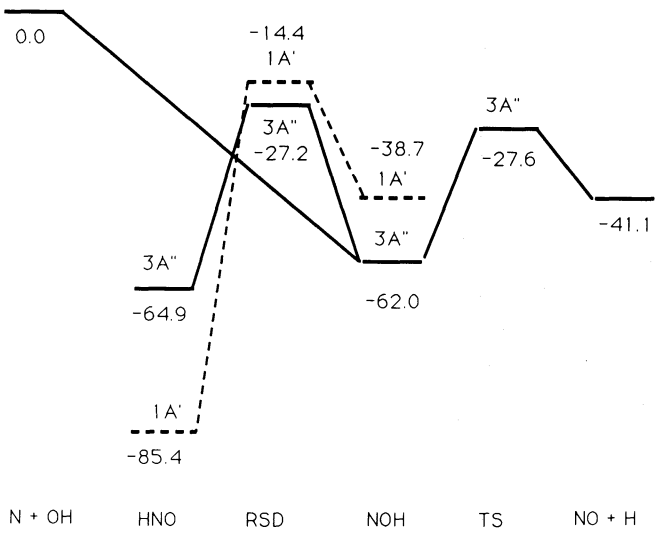

Fig. 5. Relative energetical positions of minima, transitions states and stationnary points of the three atomic system (N, O, H). Units are in kcal/mol (1 kcal $\approx$ 503 K)

Table 7a comparison of the column densities of nitric oxide and other nitrogenated molecules in L134N and TMC1. The references for the data on TMC1 are given in the table. We tried to obtain data at the same position and with the same telescope (IRAM 30m) when it was possible, but these data are less homogeneous than those of Swade (1989). Compared with L134N, the [NO]/[HCN] column density ratio in TMC1 is at least a factor ten lower than in L134N, but the [NO]/[NH_3] and [NO]/[N_2H^+] ratio may still have comparable values. The kinetic temperature, density and column density of molecular hydrogen are nearly equal in these two clouds.

The new detection of NO, and the calculation of reaction [1] give us the opportunity to run models of interstellar chemistry. As a first step, we postulated the presence of small activations barriers on reaction [1] and [2], E_{A1} and E_{A2} and studied the response of the network to the change of reaction rate. In a second step, we investigated the influence of small variations in the elemental depletions on the abundance of simple nitrogenated molecules. More generally, we will take the opportunity to discuss the chemistry of simple nitrogen molecules in cold dark clouds in view of recent developments in this area.

5.2. Models

5.2.1. Chemical reactions and cloud parameters

Reactions [1] and [2] have been studied at room temperatures and have rate constants $k_1 = 5\,10^{-11}$ cm^3 s^{-1} at 298 K (Howard & Smith 1980) and $k_2 = 3.4\,10^{-11}$ cm^3 s^{-1} in the range 196–400 K (Lee et al. 1978). As is well known, neutral–neutral reactions can play a role in interstellar chemistry as long as they do not possess activation energies; indeed barriers as low as 50 K can make most reactions totally inefficient in cold clouds.

We used the dark cloud chemical model described in Viala (1986) which deals with the steady-state chemistry of simple C–N–O bearing species (85 species and 1100 reactions). The nitrogen chemistry has been revised following the work of Pineau des Forêts et al. Furthermore, some progress has been made in the determination of reaction rate coefficients, both theoretically, by calculations on neutral–neutral reactions, and experimentally, through the study of ion-molecule reactions down to very low temperatures. Up-dated and modified chemical reactions with respect to the model presented by Viala (1986) are listed in Table 6. The only other change is the choice of elemental abundances, which is as follows: H : He : C : N : O : S : Mg : Si : Pe $= 1 : 0.1 : 3.6\,10^{-5} : 3.7\,10^{-5} : 8.5\,10^{-5} : 1.6\,10^{-9} : 3.8\,10^{-9} : 3.5\,10^{-9} : 4.7\,10^{-9}$. These are the solar system abundances reviewed by Anders & Grevesse (1989) depleted by a factor 10^4 for sulphur and the metals, by a factor 10 for carbon and oxygen and by a factor 3 for nitrogen. This choice is made in order to get the best fit to the observed chemical composition of cold dark clouds "on average": the carbon abundance is constrained by that of CO (rare isotopes) and the low metal and sulphur abundance is necessary to get a low ionisation degree so as to reproduce the observed abundances of molecular ions (HCO^+, N_2H^+...). The oxygen and nitrogen abundances can partly be constrained by the abundances of nitrogen molecules, and are considered as free parameters of the model.

We are mainly concerned to interpreting the data (Table 7) on the dark cloud L134N so that we ran models with "standard" density $n_H = n(H) + 2n(H_2) = 10^4$ cm^{-3} and temperature $T =$ 10 K, a visual extinction throughout the whole cloud of $A_V = 11$ corresponding to a total hydrogen column density $N_H = 2\,10^{22}$ cm^{-2}. The cloud (a slab of finite thickness and uniform density and temperature) is exposed to the external UV radiation field of Mathis et al. (1983); the cosmic-ray ionisation rate of H_2 is $2\,10^{-17}$ s^{-1}, and all model calculations have been performed by using a "low" electronic recombination rate for H_3^+ : $\alpha = 2\,10^{-7}\,T^{1/2}$ cm^3 s^{-1} (Adams et al. 1984).

Hereafter, unless otherwise stated, by "abundance" we mean the ratio of the column density $N(X)$ of species X to the total hydrogen column density, N_H; for dense dark clouds $N_H \approx 2N(H_2)$.

5.2.2. NO and NH_3

Figure 6 presents the computed abundance of NO as a function of the activation energies E_{A1} and E_{A2} of reactions [1] and [2]. It is clearly shown that our observed abundance in the range $5\,10^{-8}$–$1.5\,10^{-7}$ can be reproduced only if E_{A1} is less than, typically, 50 K, larger values appear excluded. In fact the best fit is obtained with essentially no activation energy on both reactions [1] and [2]. Note also the very rapid decrease of the NO abundance as E_{A1} increases only from 0 to 50 K: two orders of magnitude, and by nearly the same amount as E_{A2} decreases from 50 to 0 K. This strong sensitivity of the NO abundance on activation energies leads to fairly severe constraints on them. A more detailed analysis of Fig. 6 shows that, if there is no activation energy on reaction [1], the activation energy on reaction [2] must be less than at most 20 K; beyond this value, the computed NO abundance is between five to ten times larger than observed. If however reaction [1] has an activation energy as large as 50 K, reaction [2] must have an activation energy larger than 80· K, otherwise the NO abundance would drop up to two orders of magnitude below the observed value as E_{A2} approaches zero. In fact, if $E_{A1} = 50$ K, for $E_{A2} \geq 80$ K reaction [2] becomes negligible in destroying NO with respect to the reaction with He^+, and the NO abundance no more depends on E_{A2}.

Table 6. Up-dated and modified chemical reactions (with respect to Viala 1986)

Chemical reaction		Rate coefficient ($cm^3\,s^{-1}$)	Reference
Neutral–neutral reactions			
$C+CH$	$\rightarrow C_2+H$	$1.0\,10^{-12}$	[8]
$C+NH$	$\rightarrow CN+H$	$5.8\,10^{-12}\,T^{1/2}$	[1]
$C+OH$	$\rightarrow CO+H$	$1.0\,10^{-12}$	[8]
$C+NO$	$\rightarrow CN+O$	$5.8\,10^{-12}\,T^{1/2}$	[1]
$N+CH$	$\rightarrow CN+H$	$2.1\,10^{-11}\exp(-E_{A3}/T)$	See text
$N+CH_2$	$\rightarrow HCN+H$	$2.1\,10^{-11}\exp(-E_{A3}/T)$	See text
$N+CH_3$	$\rightarrow HCN+2H$	$2.1\,10^{-11}\exp(-E_{A3}/T)$	See text
$N+C_2$	$\rightarrow CN+C$	$2.1\,10^{-11}\exp(-E_{A3}/T)$	See text
$N+OH$	$\rightarrow NO+H$	$5.0\,10^{-11}\exp(-E_{A1}/T)$	[1]
$N+NO$	$\rightarrow N_2+O$	$3.4\,10^{-11}\exp(-E_{A2}/T)$	[1]
$O+CH$	$\rightarrow CO+H$	$1.5\,10^{-10}$	[8]
$O+NH_2$	$\rightarrow NH+OH$	$2.0\,10^{-13}\,T^{1/2}$	[1]
$O+OH$	$\rightarrow O_2+H$	$3.3\,10^{-10}\,T^{-0.4}\exp(-6/T)$	[2]
$O+CN$	$\rightarrow CO+N$	$1.0\,10^{-12}\,T^{1/2}\exp(-50/T)$	[1]
Positive-ion–neutral reactions			
$He^+ + CH_4$	$\rightarrow H^+ + CH_3 + He$	$4.8\,10^{-10}$	[9]
	$\rightarrow CH^+ + H_2 + H + He$	$2.4\,10^{-10}$	[9]
	$\rightarrow CH_2^+ + H_2 + He$	$9.0\,10^{-10}$	[9]
	$\rightarrow CH_3^+ + H + He$	$6.8\,10^{-11}$	[9]
	$\rightarrow CH_4^+ + He$	$3.4\,10^{-11}$	[9]
$He^+ + NH_3$	$\rightarrow NH^+ + H_2 + He$	$1.4\,10^{-9}\,T^{-0.42}$	[5]
	$\rightarrow NH_2^+ + H + He$	$1.4\,10^{-8}\,T^{-0.42}$	[5]
	$\rightarrow NH_3^+ + He$	$2.1\,10^{-9}\,T^{-0.42}$	[5]
$He^+ + N_2$	$\rightarrow N^+ + N + He$	$9.0\,10^{-10}$	[3]
	$\rightarrow N_2^+ + He$	$4.0\,10^{-10}$	[3]
$He^+ + H_2O$	$\rightarrow H^+ + OH + He$	$3.4\,10^{-8}\,T^{-0.94}$	[5]
	$\rightarrow OH^+ + OH + He$	$4.9\,10^{-8}\,T^{-0.94}$	[5]
	$\rightarrow H_2O^+ + He$	$1.0\,10^{-8}\,T^{-0.94}$	[5]
$He^+ + O_2$	$\rightarrow O^+ + O + He$	$8.4\,10^{-10}$	[3]
	$\rightarrow O_2^+ + He$	$8.4\,10^{-12}$	[3]
$He^+ + CO$	$\rightarrow C^+ + O + He$	$1.4\,10^{-9}$	[3]
	$\rightarrow CO^+ + He$	$1.4\,10^{-11}$	[3]
$He^+ + HCN$	$\rightarrow CN^+ + H + He$	$1.5\,10^{-9}$	[1]
	$\rightarrow CH^+ + N + He$	$6.2\,10^{-10}$	[1]
	$\rightarrow N^+ + CH + He$	$2.5\,10^{-10}$	[1]
	$\rightarrow C^+ + N + H + He$	$7.7\,10^{-10}$	[1]
$C^+ + CH_4$	$\rightarrow C_2H_2^+ + H_2$	$3.2\,10^{-10}$	[10]
	$\rightarrow C_2H_3^+ + H$	$9.8\,10^{-10}$	[10]
$C^+ + NH_3$	$\rightarrow NH_3^+ + C$	$8.3\,10^{-9}\,T^{-0.39}$	[4]
	$\rightarrow H_2CN^+ + H$	$7.8\,10^{-9}\,T^{-0.39}$	[4]
	$\rightarrow HCN^+ + H_2$	$5.0\,10^{-10}\,T^{-0.39}$	[4]
$C^+ + H_2O$	$\rightarrow HCO^+ + H$	$2.4\,10^{-7}\,T^{-0.91}$	[4]
$C^+ + O_2$	$\rightarrow O^+ + CO$	$4.8\,10^{-10} + 3.0\,10^{-13}\,T$	[11]
	$\rightarrow CO^+ + O$	$3.0\,10^{-10} + 1.9\,10^{-13}\,T$	[11]
$C^+ + HCN$	$\rightarrow C_2N^+ + H$	$4.0\,10^{-9} - 3.2\,10^{-12}\,T$	[7]
$C^+ + NO$	$\rightarrow NO^+ + C$	$3.4\,10^{-9}$	[1]
$N^+ + H_2(J=0)$	$\rightarrow NH^+ + H$	$8.3\,10^{-10}\exp(-168.5/T)$	[12]
$N^+ + H_2(J=1)$	$\rightarrow NH^+ + H$	$5.5\,10^{-10}\exp(-41.9/T)$	[12]
$N^+ + CH_4$	$\rightarrow CH_3^+ + N + H$	$4.3\,10^{-10}$	[3]
	$\rightarrow CH_4^+ + N$	$3.3\,10^{-11}$	[3]
	$\rightarrow HCN^+ + H_2 + H$	$8.2\,10^{-11}$	[3]
	$\rightarrow H_2CN^+ + 2H$	$2.6\,10^{-10}$	[3]
$N^+ + NH_3$	$\rightarrow NH_2^+ + NH$	$2.7\,10^{-9}\,T^{-0.53}$	[4]
	$\rightarrow NH_3^+ + N$	$2.5\,10^{-8}\,T^{-0.53}$	[4]
	$\rightarrow N_2H^+ + H_2$	$2.7\,10^{-9}\,T^{-0.53}$	[4]
$N^+ + H_2O$	$\rightarrow H_2O^+ + N$	$5.9\,10^{-8}\,T^{-0.54}$	[4]

Table 6 (continued)

Chemical reaction		Rate coefficient ($cm^3\ s^{-1}$)	Reference
Positive-ion–neutral reactions (continued)			
$N^+ + O_2$	$\rightarrow O^+ + NO$	$3.3\,10^{-11}$	[3]
	$\rightarrow O_2^+ + N$	$2.8\,10^{-10}$	[3]
	$\rightarrow NO^+ + O$	$2.4\,10^{-10}$	[3]
$N^+ + CO$	$\rightarrow CO^+ + N$	$8.9\,10^{-10}\,T^{-0.17}$	[3]
	$\rightarrow CO^+ + N$	$1.1\,10^{-10}\,T^{-0.17}$	[3]
$N^+ + NO$	$\rightarrow NO^+ + N$	$4.5\,10^{-10}$	[1]
	$\rightarrow N_2^+ + O$	$7.9\,10^{-11}$	[1]
$O^+ + H_2$	$\rightarrow OH^+ + H$	$1.3\,10^{-9}$	[6]
$O^+ + O_2$	$\rightarrow O_2^+ + O$	$7.7\,10^{-10}\,T^{-0.65}$	[13]
$O^+ + HCN$	$\rightarrow CO^+ + NH$	$1.4\,10^{-9}$–$7.0\,10^{-13}\,T$	[7]
	$\rightarrow HCO^+ + N$	$1.4\,10^{-9}$–$7.0\,10^{-13}\,T$	[7]
	$\rightarrow NO^+ + CH$	$1.4\,10^{-9}$–$7.0\,10^{-13}\,T$	[7]
$H_3^+ + CH_4$	$\rightarrow CH_5^+ + H_2$	$1.9\,10^{-9}$	[14]
$H_3^+ + NH_3$	$\rightarrow NH_4^+ + H_2$	$9.1\,10^{-9}$	[14]
$H_3^+ + N_2$	$\rightarrow N_2H^+ + H_2$	$1.3\,10^{-9}$	[14]
$H_3^+ + CO$	$\rightarrow HCO^+ + H_2$	$1.7\,10^{-9}$	[14]
$H_3^+ + HCN$	$\rightarrow H_2CN^+ + H_2$	$1.2\,10^{-8}$–$1.5\,10^{-11}\,T$	[7]
$CH^+ + H_2$	$\rightarrow CH_2^+ + H$	$1.5\,10^{-9}$	[6]
$CH_2^+ + N$	$\rightarrow HCN^+ + H$	$9.4\,10^{-10}$	[1]
$CH_3^+ + N$	$\rightarrow HCN^+ + H_2$	$6.7\,10^{-11}$	[1]
	$\rightarrow H_2CN^+ + H$	$6.7\,10^{-11}$	[1]
$NH_2^+ + H_2$	$\rightarrow NH_3^+ + H$	$2.7\,10^{-10}$	[1]
$NH_3^+ + H_2$	$\rightarrow NH_4^+ + H$	$2.4\,10^{-12}$	[1]
$NH_3^+ + H_2O$	$\rightarrow NH_4^+ + OH$	$2.5\,10^{-10}$	[1]
$N_2^+ + H_2$	$\rightarrow N_2H^+ + H$	$5.1\,10^{-10}\,T^{0.24}$	[1]
$N_2^+ + O_2$	$\rightarrow O_2^+ + N_2$	$2.8\,10^{-9}\,T^{-0.73}$	[13]
$N_2H^+ + CO_2$	$\rightarrow HCO_2^+ + N_2$	$1.4\,10^{-9}$	[1]
$O_2^+ + N$	$\rightarrow NO^+ + O$	$7.8\,10^{-11}$	[1]
$CO^+ + O_2$	$\rightarrow O_2^+ + CO$	$2.1\,10^{-09}$–$2.5\,10^{-12}\,T$	[11]
$HCO^+ + NH_3$	$\rightarrow NH_4^+ + CO$	$1.9\,10^{-9}$	[1]
$HCO^+ + HCN$	$\rightarrow H_2CN^+ + CO$	$5.0\,10^{-9}$–$6.3\,10^{-12}\,T$	[7]
$NO^+ + Fe$	$\rightarrow Fe^+ + NO$	$1.0\,10^{-9}$	[1]
Electronic recombination reactions			
$NH_4^+ + e^-$	$\rightarrow NH_3 + H$	$2.1\,10^{-5}\,T^{-0.6}$	[1]
	$\rightarrow NH_2 + H_2$	$2.1\,10^{-5}\,T^{-0.6}$	[1]
$C_2N^+ + e^-$	$\rightarrow C_2 + N$	$1.7\,10^{-6}\,T^{-1/2}$	[1]
	$\rightarrow CN + C$	$3.5\,10^{-6}\,T^{-1/2}$	[1]
$NO^+ + e^-$	$\rightarrow N + O$	$6.8\,10^{-5}\,T^{-0.9}$	[1]
The following reactions have been deleted from the model			
$H_3^+ + N$	$\rightarrow NH_2^+ + H$	activation barrier	[15]
$N + CN$	$\rightarrow N_2 + C$		[1]
$O + NH_2$	$\rightarrow HNO + H$		[1]
$CH_2^+ + CH_3$	$\rightarrow C_2H_2^+ + 2H_2$	endothermic	
$C_2H_2^+ + C_2$	$\rightarrow C_2H^+ + C_2H$	endothermic	
$NH_2^+ + HCO$	$\rightarrow H_2CO^+ + NH$	endothermic	
$OH^+ + NH$	$\rightarrow NH^+ + OH$	endothermic	
$H_2O^+ + CO$	$\rightarrow HCO^+ + OH$	endothermic	
$HCN^+ + O$	$\rightarrow O^+ + HCN$	endothermic	
$HNO^+ + CH_3$	$\rightarrow CH_4^+ + NO$	endothermic	
$NH_3^+ + e^-$	$\rightarrow NH + 2H$ or H_2		[1]
$H_2CN^+ + e^-$	$\rightarrow CN + 2H$ or H_2		[1]

References: [1] Pineau des Forêts et al. (1990); [2] Davidsson & Stenholm (1990); [3] Rowe et al. (1985a); [4] Rowe & Marquette (1987); [5] Marquette et al. (1985); [6] Federer et al. (1985); [7] Clary et al. (1985); [8] Graff (1989); [9] Chatham et al. (1983); [10] Bohme et al. (1982); [11] Miller et al. (1984); [12] Marquette et al. (1988); [13] Rowe et al. (1985b); [14] Marquette et al. 1989; [15] Herbst et al. (1987).

Table 7. Abundances of molecules as a function of C–N–O depletions

Molecule	TMC1	L134N	δ_C 10	10	10	10	10
$N(X)/N_H$	$N(X)/N_H$	$N(X)/N_H$	δ_N 3	1	10	10	3
			δ_O 10	10	10	3	3
NO	<3.5 (−08)	0.8–1.2 (−07)	6.0 (−08)	4.1 (−0.8)	6.5 (−08)	6.9 (−08)	6.1 (−08)
NH_3	≈2.0 (−08)	2.0–8.0 (−08)	3.3 (−08)	5.6 (−08)	1.5 (−08)	1.7 (−08)	3.8 (−08)
N_2H^+	≈3.5 (−10)	0.5–4.0 (−10)	3.9 (−10)	9.0 (−10)	1.2 (−10)	1.1 (−10)	3.4 (−10)
CN	≈1.5 (−08)	<1.0 (−09)	1.1 (−07)	2.5 (−07)	3.6 (−08)	3.0 (−09)	8.5 (−09)
HCN+HNC	≈7.0 (−08)	0.4–9.0 (−09)	2.0 (−07)	3.4 (−07)	8.7 (−08)	2.7 (−08)	5.8 (−08)
$HCNH^+$	≈9.5 (−10)	<1.6 (−09)	5.5 (−10)	7.6 (−10)	2.6 (−10)	8.8 (−11)	1.7 (−10)
$N(NO)/N(X)$							
NO/NH_3	<2.0	1.6–1.8	1.8	0.73	4.3	4.0	1.6
NO/N_2H^+	<110	190–410	150	45	540	630	180
NO/(HCN+HNC)	<0.47	6.8–11	0.3	0.12	0.75	2.5	1.1

a(−b) denotes a 10^{-b}

The data for L134N are from Swade (1989), except for NO (this work) and CN (Churchwell & Bieging (1983). The data for TMC1 are from: NO – this work, NH_3 – Olano et al. (1988), N_2H^+ – Irvine et al. (1987), CN – Churchwell & Bieging (1983), HCN and $HCNH^+$ – Schilke et al. (1991), HNC – Irvine & Schloerb (1984).

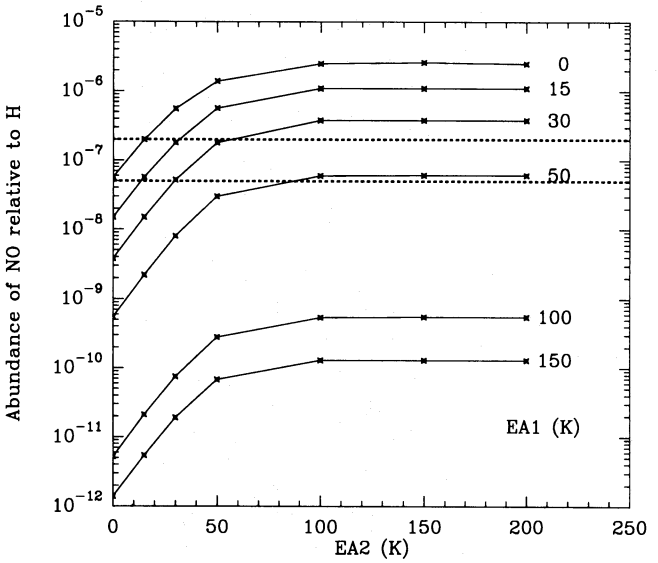

Fig. 6. Model calculations of the abundance of nitric oxide relative to hydrogen H as a function of the activation energy of the reaction destroying it, E_{A2}. Lines are drawn for several values of the activation energy of the reaction forming NO, E_{A1}. The dashed lines represent the range of observed abundance in L134N

Large values of the activation energy on reaction [2] appear, however, excluded if we consider other nitrogenated molecules, especially the nitrogen hydrides NH, NH_2 and NH_3, whose abundances as a function of E_{A1} and E_{A2} are plotted in Fig. 7. This figure corroborates the result obtained by Pineau des Forêts et al. (1990), and already mentioned, that reaction [2] initiates the gas phase production of nitrogen hydrides: the abundances of these molecules drop by factors between 10 and 100 as the activation energy of reaction [2] increases between 0 and 100 K. Beyond 100 K reaction [2] no longer plays any role in the synthesis of nitrogen hydrides. Unfortunately, among these species, only NH_3 has been observed: the abundance in the range $1–9\,10^{-8}$ derived in the dark cloud L134N, is reproduced by our model calculations ($2–3\,10^{-8}$) only if $E_{A1} \leq 15$ K and $E_{A2} \leq 50$ K. As pointed out by Le Bourlot (1991), this rather good agreement is due to the large $H_2(J=1)/H_2(\text{tot})$ ratio of the order of one percent, much higher than the expected ratio at LTE. The main differences between Le Bourlot's calculations and ours come from the act that he uses, for the reaction $N^+ + H_2$ $(J=1) \rightarrow NH^+ + H$, a rate coefficient of $8.35\,10^{-10}$ cm^3 s^{-1}, while we use a somewhat lower value of $5.55\,10^{-10}\exp(-41.9/T)$ cm^3 s^{-1}. This value has been derived from the measurements by Marquette et al. (1988) of the rate coefficient and the endothermicities of the reactions with $H_2(J=0)$ and "normal"-H_2 ["normal" H_2 corresponds to 3/4 ortho-H_2 $(J=1)$ and 1/4 para-H_2 $(J=0)$]. A direct study of the reaction with ortho-H_2 down to interstellar temperatures would be desirable.

5.2.3. N_2 and N_2H^+

The abundances of N_2 and N_2H^+ as a function of E_{A1} and E_{A2} are plotted in Fig. 8a, b, while Fig. 8c presents the abundance of N_2H^+ versus that of N_2, showing the strong linear correlation between the two species. More precisely the abundance of N_2H^+ is entirely controlled by that of N_2. Indeed, the ion is produced by the protonation reaction $H_3^+ + N_2 \rightarrow N_2H^+ + H_2$ and it is destroyed by the recombination on electrons $N_2H^+ + e^- \rightarrow N_2 + H$, which recycles N_2. The very strong correlation shown in Fig. 8c rests partly on the assumption that the cloud is homogeneous, leading to a nearly constant ionisation degree and fractional abundance of H_3^+ in the core of the cloud, so that the fractional abundance of N_2H^+ is directly proportional to that of N_2. Variations of physical parameters throughout the cloud would probably alter the constancy of the abundance ratio N_2H^+/N_2, but the correlation will persist, although not so strong. Due to this, N_2H^+ can serve as a tracer of molecular nitrogen, which is unobservable in dense clouds, and to a lesser extent, as an indicator of the abundance of nitrogen in these objects, since at

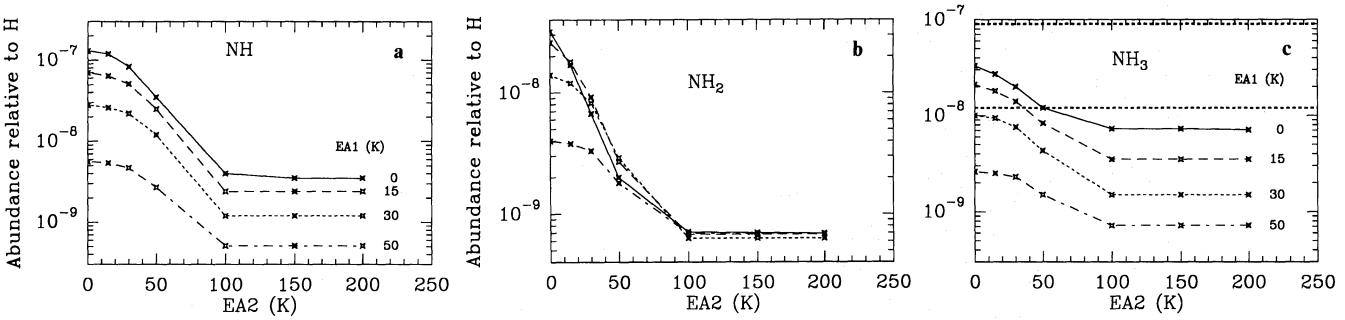

Fig. 7a–c. Abundance relative to H of **a** NH, **b** NH_2 and **c** NH_3 as function of E_{A2}. Lines are drawn for $E_{A1}=0$ (full), 15 K (dashed), 30 K (dotted) and 50 K (dot–dashed). The bold dotted lines indicate the range of ammonia abundance found in L134N

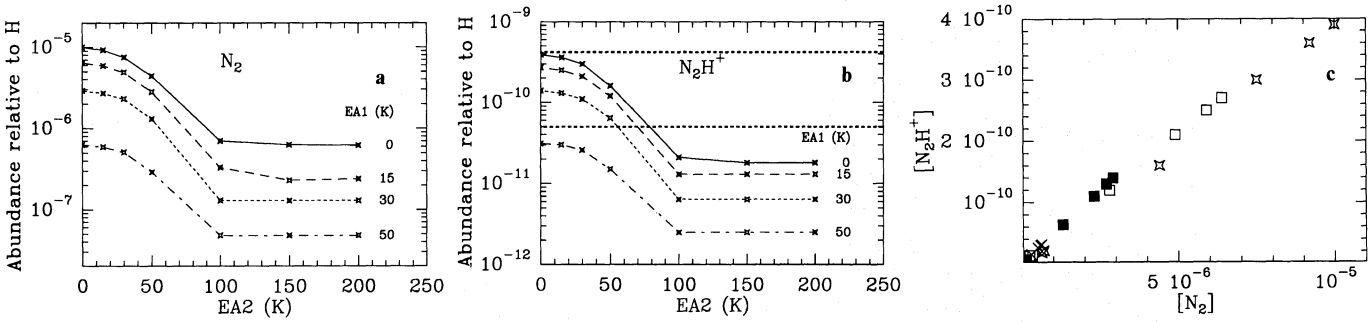

Fig. 8a–c. Abundance relative to H of **a** N_2 and **b** N_2H^+ as a function of E_{A2}. Lines are drawn for $E_{A1}=0$ (full), 15 K (dashed), 30 K (dotted) and 50 K (dot–dashed). The bold dotted lines indicate the range of N_2H^+ abundance found in L134N. **c** Relative abundance of N_2H^+ as a function of that of N_2

least 50% of gas phase nitrogen is in the form of N_2. A nitrogen abundance of $3.7\,10^{-5}$, i.e. depleted by a factor 3 with respect to the solar value, has been adopted in our model calculations so as to reproduce, as shown in Fig. 8b, the observed abundance N_2H^+ in L134N which lies in the range $0.5–5\,10^{-10}$ (Swade 1989). This agreement also requires a severe depletion of metals and sulphur, by a factor of 10^4, necessary to maintain an ionisation degree as low as $3\,10^{-8}$. This leads to a computed abundance of HCO^+ of $3\,10^{-9}$, in very good agreement with the observed value of $3.5\,10^{-9}$ reported by Swade. It may also be interesting to note that HCO^+ and H_3^+, with an abundance of $5\,10^{-9}$, are the most abundant molecular ions, as abundant as the metallic ions Mg^+, Si^+ and Fe^+.

5.2.4. CN and HCN + HNC

The last two nitrogenated molecules included in the chemical model for which observations are available are CN and HCN. *Since our model does not deal with the two different isomeric form HCN and HNC, by observed values of HCN we will in fact refer to the sum of the observed abundances of HCN and HNC, so as to be directly comparable with our computed abundance of HCN.* For L134N, Swade (1989) reports an observed abundance of HCN + HNC in the range $5\,10^{-10}–9\,10^{-9}$ whereas an upper limit of 10^{-9} for the abundance of CN is given by Irvine et al. (1987). A glance at Fig. 9, in which the computed abundances of CN and HCN are plotted as a function of E_{A1} and E_{A2}, shows clearly that the model overestimates the observations by between one and three orders of magnitude, unless the activation energy of reaction [1] is above 100–150 K, a result incompatible with that derived for the other nitrogen species discussed so far. In our chemical scheme, CN and HCN are produced by the dissociative electronic recombinations of HCN^+ and H_2CN^+ as well as by neutral–neutral reactions between atomic nitrogen and C_2, CH, CH_2 and CH_3. We have run models in which an activation energy of 100 K is assumed for all these last reactions, in which case they become negligible and electronic recombinations are the main route to both CN and HCN: this leads to reduction of the abundance of CN and HCN by factors 3 and 2 respectively. This is not enough to reproduce the observations, besides the fact it is a rather ad hoc assumption. Another evident way to reduce the CN and HCN abundances is to assume a higher depletion of nitrogen for the dark cloud L134N; all models presented so far have been computed with a nitrogen abundance depleted by factor of three with respect to solar value; with a depletion factor of ten, i.e. if the nitrogen abundance is reduced by a further factor of 3, most nitrogen bearing molecules, including CN and HCN, are reduced by the same factor. Only NO is rather insensitive to the nitrogen abundance because it is both formed and destroyed through reactions with atomic nitrogen. The reduction of the abundances of molecules like NH_3 and N_2H^+ remains compatible with the observations (see Figs. 5 and 6). With computed values $x(CN)\sim 4\,10^{-8}$ and $x(HCN)\sim 8\,10^{-8}$, the discrepancy with observations is reduced, but the CN and HCN abundances remain too high to reproduce the observations in L134N. It must be noted however that these computed abundances are in fairly

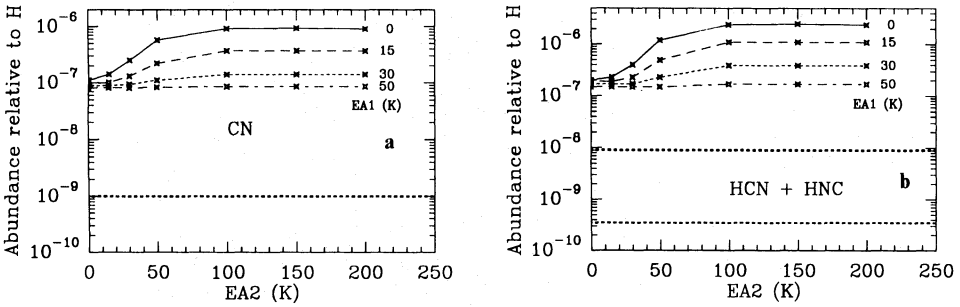

Fig. 9a and b. Abundance relative to H of **a** CN and **b** HCN+HNC as a function of E_{A2}. Lines are drawn for $E_{A1}=0$ (full), 15 K (dashed), 30 K (dotted) and 50 K (dot–dashed). The bold dotted lines indicate the range of abundances found in L134N

good agreement with the abundances observed in the dark cloud TMC1, $x(CN) \leq 1.5\,10^{-8}$ (Irvine et al. 1987) and $x(HCN+HNC) \sim 8\,10^{-8}$ (Schilke et al. 1991; Irvine & Schloerb 1984), which is well known to exhibit large amount of nitrogenated hydrocarbons. The comparison between the model and the observations is particularly difficult for CN for two reasons: (1) due to the very low excitation temperature of the CN rotational transitions, 3–4 K (Crutcher et al. 1984), the lines are both weak and saturated so that the derived column densities are fairly unprecise; (2) CN is present in the external parts of the cloud where the model density and temperature should be respectively lower and higher than in the core.

5.2.5. Variations of elemental depletions

The differences observed for the abundances of NH_3 and C–N bearing species between L134N and TMC1, two dark clouds of apparently the same global properties, is a well known problem of interstellar chemistry not satisfactorily solved. Large amounts of these species are computed in the early evolution of time-dependent chemical models (e.g. Herbst & Leung 1989) and can be invoked to explain the observations in TMC1. Furthermore, dynamical mixing is able to maintain such large abundances over longer periods (Chièze et al. 1991). By the way, this also indicates that the lower abundances (a factor 50 for CN and 100 for HCN+HNC) computed in steady state would better apply to L134N. The problem remains since these lower steady-state abundances are still too high. Hence, differences in elemental abundances between the two clouds appears to be the simplest remaining explanation to be proposed. The influence of the C–N–O depletion on the chemical composition of interstellar clouds has recently been studied by Pineau des Forêts et al. (1991), while Langer & Graedel (1989) more specifically studied the influence of the C/O ratio of elemental abundances. We present in Table 7 the abundances we have computed for different C–N–O depletions noted as δ_C, δ_N and δ_O; all models have a metal and sulfur depletion of 10^4, no activation barrier on the neutral–neutral reactions mentioned above, and the physical parameters indicated at the beginning of this section. As can be seen in the table, and shown in other model calculations such as those by Langer & Graedel, the abundance of CN and HCN decreases with increasing oxygen abundance. It is however difficult to lower them to the values reported for L134N, unless the depletion of nitrogen is larger than 10, which is incompatible with the observations of other nitrogenated molecules, especially N_2H^+, or the oxygen is nearly undepleted, an improbable hypothesis because a notable fraction of oxygen must be tied up in grains. The main conclusion is that our simple steady-state chemical model fails to reproduce simultaneously the abundances of the simplest nitrogenated molecules observed in the dark cloud L134N, whereas it appears more easy to do so for the similar cloud TMC1. It also seems that the relaxation of the steady-state assumption will make things worse. A more sophisticated model, which is beyond the scope of the present paper, appears necessary. Measurement of the actual abundance of the ion $HCNH^+$ in L134N, instead of the upper limit only available up to now (Schilke et al. 1991), would also provide useful constraints on chemical models.

6. Conclusions

The main conclusions of this work can be summarized as follows:

— Nitric oxide is a fairly abundant interstellar species in dark and warm clouds, with an abundance comparable to that of $C^{18}O$.

— The abundance of NO which we derive for the dark cloud L134N, together with observations of some other simple nitrogen bearing species reported elsewhere, have been analysed with a steady-state chemical model that includes gas phase reactions alone and takes into account the chemical reaction scheme proposed by Pineau des Forêts et al. (1990). As proposed by these authors, we investigated the influence of activation barriers on reactions:

$$[1]\ N+OH \rightarrow NO+H \quad \text{and} \quad [2]\ N+NO \rightarrow N_2+O.$$

— Quantum mechanics calculations show that reaction [1] has no activation barrier, or a very low one, within the error bar of these calculations (less than a few tens of Kelvins); this also implies that the existence of NOH ($^3A''$) cannot be excluded in molecular clouds.

These calculations give a reaction barrier on the exit channel to NO, easily overcome from N+OH but forbidding the reverse reaction.

Other routes to HNO from N+OH, via isomerization or spin-orbit coupling are calculated to be negligible.

— The observed abundance of NO in L134N is well reproduced if NO is mainly formed by the neutral–neutral reaction [1]. This reaction must have no activation barrier, or a very low one, typically less than 50 K as supported by theoretical calculations.

— The neutral–neutral reaction [2] must have no activation energy either. Indeed, it is the main destruction process of NO and it initiates the gas phase chemistry of ammonia and other nitrogen hydrides. If reaction [1] has no activation energy, an activation barrier on reaction [2], even small, would lead to too large an NO abundance and would impede the formation of

other nitrogenated species. The observed abundance of ammonia is reproduced by the model.

— The nitrogen available in the gas phase is shared equally among the atomic and molecular forms. The depletion of nitrogen with respect to the solar system abundance must be small, at most a factor 3, to reproduce the observations of the molecular ion N_2H^+.

— The abundances of this ion and of the other observed molecular ion HCO^+ require a very low ionisation degree, around 10^{-8}, in the core of the cloud which implies a strong metal depletion by at least a factor 10^4.

— It is almost impossible, with the same model, to reproduce simultaneously the abundances of all simple nitrogenated molecules and molecular ions observed in the dark cloud L134N.

Acknowledgements. We thank the IRAM staff at Pico Veleta (Spain) for the telescope operations. This work was partly supported by the CNRS-GDR "Physicochimie des molécules interstellaires". Model calculations have been performed at the Centre Inter Régional de Calcul Electronique (CIRCE), Orsay France.

References

Adams N., Smith D., Alge E., 1984, JCP 81, 1778
Anders E., Grevesse N., 1989, Geochemica et Cosmichimica Acta 53, 197
Bennett R.J.M., 1970, MNRAS 147, 35
Blake G.A., Sutton E.C., Masson C.R., Phillips T.G., 1986, ApJS 60, 357
Bohme D.K., Rakshit A.B., Schiff H.I., 1982, Chem. Phys. Lett. 93, 592
Brasseur G., Nicolet M., 1973, Planet. Space Sci. 21, 939
Bruna P.J., Marian C.M., 1979, Chem. Phys. Lett. 67, 109
Bruna P.J., 1980, Chem. Phys. 49, 39
Chatham H., Hils D., Robertson R., Gallagher A.C., 1983, JCP 79, 1301
Chieze J.-P., Pineau des Forêts G., Herbst E., 1991, ApJ 373, 110
Churchwell E., Bieging J.H., 1983, ApJ 265, 216
Clary D.C., Smith D., Adams N.G., 1985, Chem. Phys. Lett. 119, 320
Clyne, McDermid, 1974, JCP 75, 2800
Dalby F.W., 1958, Can. J. Phys. 36, 1336
Davidsson J., Stenholm L.G., 1990, A&A 230, 504
Federer W., Villinger H., Tosi P., Bassi D., Lindinger W., 1985, in: Dierksen G.H.F., Huebner W.F., Langoff P.W. (eds.) Molecular Astrophysics. Reidel, Dordrecht, p. 649
Frerking M.A., Langer W.D., Wilson R.W., 1982, ApJ 262, 590
Gallagher J.J., Johnson C.M., 1956, Phys. Rev. 103, 1727
Gerin M., Bel N., Combes F., Viala Y.P., 1990, in: Molecular Clouds, Manchester Conference
Graff M.M., 1989, ApJ 339, 239
Graff M.M., Dalgarno A., 1987, ApJ 317, 432
Ha Tae-Kyu, Cimiraglia R., 1982, Mol. Phys. 45, 1095
Heiberg A., Almlof J., 1982, Chem. Phys. Lett. 85, 542
Herbst E., deFrees D.J., McLean A.D., 1987, ApJ 321, 898
Herbst E., deFrees D.J., Talbi D., Pauzat F., Koch W., McLean A.D., 1991, J. Chem. Phys. 94, 7842
Herbst E., Klemperer W., 1973, ApJ 185, 505
Herbst E., Leung C.M., 1989, ApJS 69, 271
Herzberg G., 1950, Molecular Spectra and Molecular Structure. I. Spectra of Diatomic Molecules Van Nostrand, New York, Toronto, London
Howard M.J., Smith I.W.M., 1980, Chem. Phys. Lett. 69, 40
Irvine W.M., Goldsmith P.F., Hjalmarson A., 1987, in: Hollenbach D.J., Thronson H.A. (eds.) Interstellar Processes. Reidel, Dordrecht, p. 561
Irvine W.M., Schloerb F.P., 1984, ApJ 282, 516
Langer W.D., Graedel J.E., 1989, ApJS 69, 241
Le Bourlot J., 1991, A&A 242, 235
Lee J.H., Michael J.V., Payne W.A., Stief L.J., 1978, JCP 69, 3069
Lengsfield B.H.III, 1980, JCP, 73, 382
Lengsfield B.H.III, Liu B., 1981, JCP 75, 478
Lis D.C., Goldsmith P.F., 1989, ApJ 337, 704
Liszt H.S., Turner B.E., 1978, ApJ 224, L73
Liu B., Yoshimine M., 1981, JCP 74, 612
MacGonagle D., Ziurys L.M., Minh Y., Irvine W.M., 1990, ApJ 359, 121
McLean A.D., Loew G., Berkowicz D.S., 1977, J. Mol. Spectro. 64, 184
Marquette J.B., Rebrion C., Rowe B.R., 1988, JCP 89, 2041
Marquette J.B., Rebrion C., Rowe B.R., 1989, A&A 213, L29
Marquette J.B., Rowe B.R., Dupeyrat G., Poissant G., Rebrion C., 1985, Chem. Phys. Lett. 122, 431
Mathis J.S., Metzger P.G., Panagia N., 1983, A&A 128, 212
Mauersberger R., Guélin M., Martin-Pintado J., et al., 1989, A&AS 79, 217
Miller T.M., Wetterskog R.E., Paulson J.F., 1984, JCP 80, 4922
Olano C.A., Walmsley C.M., Wilson T.L., 1988, A&A 196, 194
Pineau des Forêts G., Roueff E., Flower D.R., 1990, MNRAS 244, 668
Pineau des Forêts G., Flower D.R., Millar T.J., 1991, MNRAS 253, 217
Poynter R.L., Pickett H.M., 1984, JPL Publication 80–23, revision 2
Pwa T.H., Pottasch S.R., 19XX, A&A 164, 116
Rowe B., Marquette J.B., 1987, Int. J. Mass Spectrom. Ion Proc. 80, 239
Rowe B., Marquette J.B., Dupeyrat G., Ferguson E.E., 1985a, Chem. Phys. Lett. 113, 403
Rowe B., Marquette J.B., Dupeyrat G., 1985b, in: Dierksen G.H.F., Huebner W.F., Langoff P.W. (eds.) Molecular Astrophysics. Reidel, Dordrecht, p. 561
Saleck A.H., Yamada K.M.T., Winnewisser G., 1991, Molec. Physics 72, 1135
Schilke P., Walmsley C.M., Millar T.J., Henkel C., 1991, A&A 247, 487
Schloerb F.P., Snell R.L., 1984, ApJ 283, 129
Strobel D.F., 1971, J. Geophys. Res. 76, 8384
Swade D.A., 1989, ApJ 345, 828
Tatum J.B., 1986, ApJS 60, 433
Ulich B.L., Hollis J.M., Snyder L.E., 1977, ApJL 217, L105
Viala Y.P., 1986, A&AS 64, 391
Walch S.T., Rohlfing C.M., 1990, JCP 91, 2939
Wilson T.L., Serabyn E., Henkel C., Walmsley C.M., 1986, A&A 158, L1
Ziurys L.M., Mac Gonagle D., Minh Y., Irvine W.M., 1991, ApJ 373, 535